Electrostatic self-assembled graphene oxide-collagen scaffolds towards a three-dimensional environment for biomimetic applications

André F. Girão[1], Gil Gonçalves[1], Kulraj S. Bhangra[2], James B. Phillips[2], Jonathan Knowles[2], Gonzalo Hurietta[1], Manoj K. Singh[1], Igor Bdkin[1], António Completo[1], Paula A. A. P. Marques[1,*]

[1]TEMA, Department of Mechanical Engineering, University of Aveiro, 3810-193 Aveiro, Portugal

[2]Department of Biomaterials and Tissue Engineering, UCL Eastman Dental Institute, University College London, 256 Gray's Inn Road, London WC1X 8LD, UK

Abstract

In light of the importance of collagen, one of the most abundant proteins in mammals, the preparation of collagen-based scaffolds is gaining interest in the field of tissue engineering. However, there is a need to develop strategies to produce collagen three dimensional structures with mechanical properties suitable for proper handling and manipulation. In this work, the feasibility of combining graphene oxide (GO) with collagen was explored, with a view to providing structural reinforcement to collagen-based scaffolds and concomitantly add a positive influence to the cells conduct. We report a self-assembled GO-collagen (GO-Col) scaffold with a porous network resulting from preferential interaction of oxygen functional groups located on the GO nanosheet

edges with amine groups on the biopolymer chain. Such conjugation was characterized and explored minutely, as well as its influence on the structural properties of the scaffolds that proved to be highly dependent on the pH of the medium and the collagen/GO weight ratio used during the synthesis. Indeed, accurate control of those variables was shown to modulate the repulsion and bonding forces within the GO-Col nanocomposite system, providing the opportunity to fabricate a wide range of stable GO-Col scaffolds. The most viable candidate in terms of mechanical integrity was selected and tested together with its reduced counterpart concerning its stability in physiological medium under mechanical stimulation. The cytocompatibility of these two scaffolds was tested by culturing Schwann cells on the materials surfaces for 24 h. The results indicated that these novel scaffolds provide a useful new approach for the assemblage of suitable cellular microenvironments that could be explored on tissue engineering applications.

Keywords: graphene oxide, collagen, scaffold, self-assembled hydrogel, , Schwann cell, cytocompatibility , tissue engineering.

1. Introduction

The wide range of commercial, industrial and scientific applications potentially provided by two-dimensional carbon nanomaterials has placed graphene at the forefront of research in biomedicine[1] and electronics.[2] Graphene is a monolayer of sp^2 hybrid-bonded carbon atoms arranged to form a honeycomb structure, providing excellent electrical and thermal conductivities, high mechanical strength and remarkable optical properties.[3] Graphene can be directly obtained by using either a bottom-up approach via chemical vapor deposition (CVD)[4] or a top-down strategy like mechanical exfoliation of graphite; an indirect route involving chemical exfoliation of graphite to graphene oxide (GO) followed by reduction is common due to high yield and low-cost.[5] GO presents a similar layered structure to graphene, but its carbon sheets are heavily oxygenated with hydroxyl and epoxy functional groups on the basal plane and carbonyl/carboxylic acids groups on the plane edges. These functional groups are responsible for making the GO surface highly hydrophilic, which facilitates the formation of stable aqueous colloids.[6, 7] In addition to the formation of graphene-like sheets through the reduction of GO by eliminating surface oxygenated moieties originating the so-called reduced GO (rGO), GO also offers the possibility of combining those oxygen-containing groups with specific functional groups on biomolecules or other polymers. This can be via either covalent (e.g. nucleophilic substitution) or non-covalent (e.g. Van der Waals forces, electrostatic interaction, hydrogen bonding) methods and can be used to adapt and improve materials.[8-10]

Recently, GO has received much interest in the field of regenerative medicine and studies have shown that it can positively influence the attachment, proliferation and differentiation of stem cells[11-14]. Lee *et al.*,[15] reported that the different binding

interactions established between graphene and GO films with insulin could influence the routes of the osteogenic differentiation of mesenchymal stem cells (MSCs). They concluded that the π-π interaction provided by graphene caused suppression of adipogenesis due to insulin denaturation, whereas GO was able to encourage differentiation of MSCs to adipocytes due to the electrostatic binding interaction. In other examples, the adhesion, proliferation and differentiation of induced pluripotent stem cells (iPSCs) were studied using both graphene and GO substrates.[12] The results showed that the graphene substrate was able to maintain iPSCs in an undifferentiated state for longer periods of time and that proliferation and differentiation occurred faster on GO substrates.

GO has been shown to enhance the bulk properties of materials such as poly-L-lysine[16] and polycaprolactone,[17] forming GO composites that are able to successfully mimic complex cellular microenvironments. In fact, GO based composites can present a range of forms including films[18], electrospun fibres[19] and hydrogels[20]. From a biomedical perspective, physically cross-linked hydrogels are particularly attractive due to their ability to mimic living-tissue, but also because of their simple synthesis and absence of potentially toxic chemical crosslinking agents. For instance, conductive polymers such as polypyrrole can be self-assembled with GO in order to form composite hydrogels with enhanced mechanical, electrical and electrochemical properties.[21] In other examples, electrostatic interactions and H-bonding between GO and poly(vinyl alcohol) (PVA) were explored with the purpose of creating smart GO-PVA composite hydrogels able to control the release of drugs by adapting their gel – solution transition to the pH level of the environment. [22] A similar application was explored by Piao *et al.*,[23] who studied the gelation process between GO and gelatin. They concluded that by varying the pH of the culture medium and consequently the protonation of the functional groups

of both GO and gelatin, the bonding – repulsion forces of the system could be changed and therefore the composite hydrogel behavior modulated. Indeed, the protonation of the functional groups of both GO (oxygen functionalities) and gelatin (oxygen and amine functionalities) boosted not only the formation of H-bonds but also the electrostatic attraction between negatively charged GO sheets and positively charged gelatin particles, increasing binding forces and subsequent maintenance of the gel state. Comparable GO-protein composite hydrogels were fabricated using hemoglobin[24] and chitosan[25] as GO sheets crosslinkers.

Indedd, various proteins have been used to create GO composite hydrogels, but the potential of collagen as GO crosslinker has not yet been thoroughly investigated. Collagen is the principal extracellular matrix component for many tissues and the most commonly used biomaterial in regenerative medicine applications.[26] Collagen is widely used in tissue engineering since it can easily form a hydrogel structure at physiological pH capable of simulating the extracellular matrix.[27] Additionally, collagen can be successfully integrated in hybrid networks with other materials including GO in order to enhance the biocompatibility and biodegradability of the system. For example, GO was successfully used as reinforcement agent in a collagen-gelatin composite film for enhanced wound healing.[28] In other reports, GO was combined with poly(lactic-co-glycolic acid) and collagen in order to improve the hydrophilicity and mechanical properties of a composite electrospun scaffold capable of improving attachment, proliferation and myogenic differentiation of C2C12 skeletal myoblasts.[29] A different strategy was followed by Kang *et al*.,[30] who covalently bonded the carboxylic groups located on the surface of GO flakes to the amine functional groups positioned on a collagen sponge via a carbodiimide crosslinker. It was reported that the GO addition promoted osteogenic differentiation of human MSCs, not only by enhancing the

mechanical properties of the scaffold, but also by improving its ability to adsorb proteins in the medium. The mechanical and biological properties of collagen scaffolds were also modulated by adding either GO or rGO coatings, resulting in changes to surface structure, compressive strength and cell ingrowth.[31] It was reported that the dissimilar bioactivities of the final scaffolds were significantly influenced by the specific properties of each additive, therefore, GO-Col scaffolds and their reduced counterparts present an interesting opportunity for controlling cell-material interactions.

In this work the electrostatic interactions between negatively charged GO nanosheets and positively charged collagen polymeric chains responsible for the formation of a self-assembled hydrogel were pioneeringly studied by X-ray photoelectron spectroscopy (XPS) and Atomic Force Microscopy (AFM) analysis. Our experimental studies showed that the structural network stability of the nanocomposite was dependent on the medium pH and the collagen/GO weight/weight (w/w) ratio used during the hydrogel synthesis. Therefore, by varying those experimental parameters it was possible to synthesize a wide range of GO-Col nanocomposite hydrogels. Evaluation of their mechanical and swelling properties after lyophilization showed that a stable nanocomposite was obtained using pH 2 and a 24% collagen/GO w/w ratio. The potential for this optimized GO-Col nanocomposite and its reduced counterpart to act as scaffolds for tissue engineering able to be mechanical stimulated under in vitro conditions was evaluated.

2. Experimental methods

Synthesis of the GO-Col hydrogels

A GO aqueous dispersion (4.0 mg mL^{-1}, water dispersion: Graphenea) was directly mixed with rat tail type I collagen (2.16 mg mL^{-1} protein in 0.6% acetic acid: First Link

Ltd, West Midlands, UK) and then rapidly shaken for 10 s to form a hydrogel. Different collagen/GO w/w ratios were used. Before shaking, the pH level of the reaction was controlled by adding a few drops of 1 mol dm^{-3} NaOH solution into the GO suspension until the desired pH value was reached (2, 4 or 6). The pH values were confirmed by pH test strips (Filtres Fioroni Company, Ingré, France). Several combinations were tested and the final GO-Col hydrogels were identified as "*a.b*", where *a* is the pH of the medium and *b* is the weight % of collagen relative to GO used during the hydrogel synthesis. For example, 2.24 GO-Col indicates a medium pH of 2 and a collagen weight % of 24 relative to GO.

Preparation of the GO-Col scaffolds

After synthesis, the GO-Col hydrogels were freeze-dried by lyophilisation (Telstar lyoQuest HT-40, Beijer Electronics Products AB, Malmoe, Sweden) at -80 ºC in order to obtain three dimensional (3D) porous structures. The lyophilized samples were then washed in MilliQ water for 12 h to neutralize the system and remove any impurities. Finally, the samples were freeze-dried again and the resulting 3D structures were named "*a.b GO-Col scaffolds*".

The 2.24 GO-Col scaffold composition was selected for further studies since this composition exhibited the most appropriate structural integrity. It was renamed as simply GO-Col scaffold. A reduced version of this scaffold (rGO-Col scaffold) was prepared by immersion in a hydrazine solution (1µL mL^{-1} of MilliQ water) for 24 h and intensively washed with MilliQ water to remove any hydrazine residues before freeze-drying.

Materials characterization

A digital instrument MultiMode Scanning Probe Microscope (SPM) with a Nanoscope IIIA controller in contact friction mode was used for the AFM measurements. The zeta potential and the particle size of GO and collagen suspensions at different pH values (2, 4, 6 and 8) were measured using a Zetasizer Nano ZS90 analyser (Malvern Instruments, Malvern, UK). The conformational changes of collagen with increasing pH were evaluated by an UVmini-1240 UV/visible scanning spectrophotometer (Shimadzu Scientific Instruments, Kyoto, Japan).

Both the swelling properties of scaffolds and their structural resistance in water were evaluated by immersing the samples into MilliQ water at room temperature for periods of 1 h and 24 h. The swelling ratio was calculated with the following equation:

$$\text{Swelling ratio (mg/mg)} = \frac{(W_s - W_d)}{W_d}$$

where W_s and W_d are the weights of the scaffolds at swollen and dry states, respectively. Triplicate measurements were carried out for every sample.

The compressive properties of the scaffolds in dry and wet states were tested using a Shimadzu MMT-101N (Shimadzu Scientific Instruments, Kyoto, Japan) with a load cell of 100 N. The cylindrical shaped samples were compressed at a rate of 2 mm min^{-1} up to the maximum limit. Three specimens with dimensions 5 mm diameter x 5 mm of thickness were used for each test condition. The compressive moduli of the samples were calculated by the analysis of the stress – strain curves, specifically, from the slope at low strain (0-15 %). For fatigue tests, the specimens immersed in Dulbecco's Modified Eagle's Medium (Sigma-Aldrich Corporation), were submitted to a 0.2 Hz sinusoidal compression of 5 % strain load up to 20000 cycles at room temperature. The stress amplitude was calculated with the following equation:

$$\textit{S}\text{tress amplitude (Pa)} = \frac{(\sigma_{max} - \sigma_{min})}{2}$$

where σ_{max} and σ_{min} are respectively the maximum and minimum stress levels measured during one cycle.

XPS was used to characterise the elemental composition of the samples. XPS spectra were acquired in an ultra high vacuum (UHV) system with a base pressure of $2x10^{-10}$ mbar. High resolution spectra were recorded at normal emission take-off angle and with a pass-energy of 20 eV, which provides an overall instrumental peak broadening of about 0.5 eV. XPS spectra were calibrated in binding energy by referencing to the first component of the C 1s core level at 284.5 eV (C sp^2). Complementary, the chemical structure of the scaffolds were analysed via attenuated total reflectance fourier transform infrared (ATR-FTIR) in a Bruker Tensor 27 FT-IR spectrometer (Bruker Corporation, Massachusetts, USA). The spectra were recorded between 4000 and 400 cm^{-1}, with a resolution of 4 cm^{-1} and 256 scans.

The microstructure of the scaffolds was evaluated using a scanning electron microscope (SEM) Hitachi SU 70 (Hitachi High-Technologies Corporation, Krefeld, F.R., Germany) and the dimensions of the pores were determined by direct analysis of ten SEM pictures.

Cytocompatibility of the scaffolds

Scaffolds with a cylindrical shape, dimensions 6 mm (diameter) x 4 mm (thickness), were tested. Samples were washed in sterile culture media Dulbecco's Modified Eagle's Medium (DMEM; Gibco) supplemented with 10% (v/v) foetal bovine serum (FBS) (Gibco) and Penicillin Streptomycin (10000 U/mL; Life Technologies) for 15 minutes. Each material was placed in a well of a 48-well plate and seeded with $1x10^4$ rat Schwann cells (SCL 4.1/F7) suspended in 500 µL culture media. Cells were added to the top of the materials and incubated for 30 minutes at 37°C and 5% CO_2 to allow the

cells to settle, then an additional 500 µL culture media was added prior to incubation for a further 24 h. Live/dead analysis was performed using Syto®-9 (5µM) and Propidium Iodide (PI) (20 µg/mL) and samples were viewed immediately after staining. The cell survival and death was determined by calculating the average of three random fields of view per sample using a fluorescence microscope (Leica DMIRB) with a 20x objective, where each field of view had an area of 0.23 mm^2. Statistical analysis was performed using Graphpad Prism 6.0 (GraphPad Software, Inc., San Diego, CA) with one-way ANOVA.

Fluorescence microscopy and SEM were used to evaluate cell attachment and morphology. The actin filaments and nuclei were fluorescently stained using phalloidin conjugated to Alexa Fluor® 488 and PI, respectively. Specimens were briefly washed in phosphate buffered saline solution (PBS) then fixed overnight at 4 °C in 4 % paraformaldehyde. Cell permeabilisation was performed using 0.5% Triton-X (Sigma-Aldrich Corporation) for 20 minutes then washed three times with PBS. A 2.5 % solution of phalloidin methanolic stock solution (Life Technologies) in PBS was added to each specimen for 20 minutes at room temperature in a dark environment. After three washes with PBS, the specimens were counter-stained using 20 µg/mL PI for 10 minutes at room temperature. Specimens were washed twice in PBS before viewing and capturing images using a Zeiss Axio Lab A1 fluorescence microscope equipped with an AxioCam ICm1 camera (Zeiss AX10, Germany). Images of the phalloidin and PI staining were superimposed using ImageJ (version 1.49v).

Additional samples were prepared for SEM by fixation in 3% glutaraldehyde for 24 h followed by sequential dehydration in 50 %, 70 %, 90 % and 100 % ethanol for 10 minutes each and lastly drying in hexamethyldisilazane for 2 minutes. Following this,

samples were carefully mounted on aluminum stubs using carbon tape. The specimens were then sputter-coated with gold and imaged using SEM (Philips XL30 FEG-SEM; FEI, Eindhoven, Netherlands) with an accelerating voltage of 10 kV and a working distance of 10 mm.

3. Results and discussion

3D self-assembly of the GO-Col hydrogels

The GO-Col hydrogels were successfully prepared by self-assembly of initially randomly dispersed GO sheets and collagen in aqueous medium. As mentioned earlier, the collagen and GO solutions were directly mixed and then shaken vigorously for a few seconds in order to get a homogeneous hydrogel. It was noticed that the gelation process only occurred at specific collagen/GO weight ratios and it was dependent of the pH of the medium (see Figure S1 in Supporting Information). Indeed, a uniform and consistent gelation only occurred for collagen / GO (w/w %) ranges between 18 and 24 for pH 2; 12 and 24 for pH 4; 6 and 12 for pH 6. It was also observed that although some of GO-Col mixtures lost some of their fluidity and become viscous for collagen/GO weight ratios below their particular gelation range, a robust 3D network was not formed since those samples were not able to pass the tube inversion test. On the other hand, when collagen/GO weight ratios higher than the particular gelation range were used, the GO sheets precipitated into several heterogeneous hydrogel clusters due to the excess of collagen adsorbed on their surfaces, weakening the crosslinking effect.

The 3D self-assembly process behind the formation of the GO-Col composite hydrogels is intimately related to the manipulation of the network of repulsive and attractive forces among the acidified GO sheets and collagen molecules, which present, respectively, a typical GO flake morphology and a fibrillar conformation according to the AFM analysis (see Figure 1 a-b). Indeed, it is the capability of the positively charged collagen

chains to act as crosslinkers between the GO sheets that originates the hydrogel (see Figure 1c), which, after lyophilization, allows the formation of a stable microporous foam (see Figure 1d). The development of GO based hydrogels originated by several supramolecular interactions including hydrogen bonding, ?coordination?, electrostatic interaction and π-π stacking was reported by other groups, opening the possibility to prepare composite hydrogels using biomacromolecules as physical crosslinkers of GO sheets.[24, 25, 32, 33]

In the present work, XPS analysis (see Figure 1e) allowed us to confirm that such interactions were mainly governed by ionic bonds between the highly electronegative charged oxygen functional groups (carboxylic acids) of GO and the protonated amine groups presented on collagen. The spectra shown in the left part of Figure 1e shows a comparison between the normalized C 1s core levels obtained for GO, collagen and GO-Col samples. These individual XPS spectra of GO and collagen are presented respectively in Figures S2a and S2b in the Supporting Information, for a better visualization. GO presents the main characteristic components at 284.5 eV (C-C) and 286.5 eV (C-O) followed by a broad component centered at 287.6 eV that can be associated with other oxygen species such as C=O and O-C=O. [30] In the case of collagen, its spectrum can be fitted by three main components centered at 284.5 eV (C-C), 285.7 eV (C-N) and 287.6 eV (C=O).[30] Importantly, in GO the highest intensity corresponds with the second component while in the case of collagen the first component, at lower binder energy (BE), dominates the spectra. In the spectrum of the GO-Col hydrogel (see Figure 1e) two broad features centered at 284.5 eV and 286.5 eV are present with similar intensities. These two main features are aligned (see the green arrows in Figure 1e, left spectra) with the main peaks detected for collagen and GO samples, respectively. Therefore, by directly comparing GO, collagen and GO-Col XPS

spectra altogether, the relative increase of the intensity of the first component (lower BE) with respect to the second one in the GO-Col spectrum strongly suggest that the collagen has successfully interacted with the GO matrix. Furthermore, since nitrogen species are characteristic of collagen, N 1s core level characterized by XPS can bring some light on the interaction between collagen and GO. As expected, N 1s XPS spectra of collagen revealed the typical C-N peak centered at 399.6 eV (see Figure 1e, right spectra).[34] After the self-assembly process with GO, an additional peak appeared at 401.5 eV, which is attributed to the ionic bonds between the protonated amine groups from collagen and the anionic carboxylic groups from GO.[35] This result confirms the electrostatic nature of the bonds between GO sheets and collagen molecules.

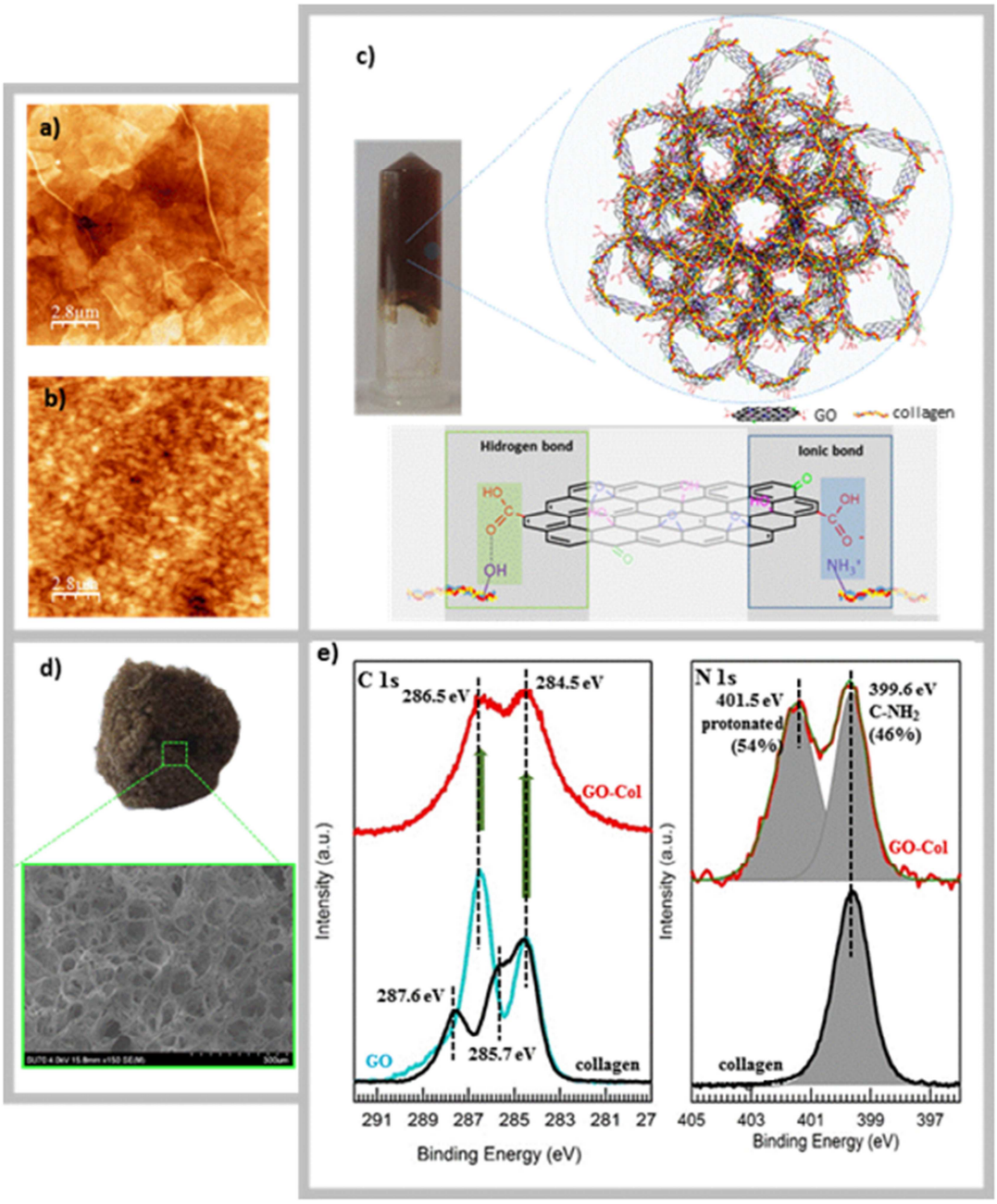

Figure 1. AFM images of individual components of the hydrogel: (a) GO sheets and (b) collagen; c) Representative photographic image of the hydrogel, together with a schematic representation of the proposed self-assembly of the GO sheets with the collagen molecules due to the establishment of different non-covalent chemical bonds; d) Photograph of GO-Col scaffold after lyophilization and the respective SEM image showing the microporous network; e) High resolution XPS of C 1s core level (left) of GO nanosheets (light blue), collagen (black) and GO-Col (red); high resolution XPS of

N 1s (right) obtained for collagen (black) and GO-Col (red) samples. The intensity of XPS spectra were normalized for doing a clear comparison.

In order to better understand the nature of the GO and collagen interactions that prompts de formation of the hydrogel, several GO and collagen solutions were prepared at different medium pH values (see Figure 2a-b). The zeta potential results confirmed that GO presents an increasingly negative charge for the pH range from 2 to 8 (see Figure 3c). This can be explained by the deprotonation of the carboxylic groups positioned on the edges of the sheets.[36] Similarly, for pH values below its isoelectric point (pH = 8), collagen exhibited a progressively weaker cationic behavior since the amino groups located along the polymer chains gradually deprotonate as the pH of the medium increases. Therefore, the attraction between the two opposite charged components and consequently the weakening of the repulsion forces among GO sheets is optimized for lower pH values.

The efficiency of collagen as a crosslinker is also related to its ability to establish hydrogen bonds (H-bonding) with the GO functional groups and consequently enhance the bonding forces among the negatively charged GO sheets. Similarly to chitosan[25] and gelatin[23], collagen has several amine and hydroxyl groups positioned along its polymeric chain that can form hydrogen bonds with the oxygenated moieties located on the GO surface (carboxyl and hydroxyl). Additionally, the epoxy groups located on the GO network can also interact with the amino functionalities of collagen by nucleophilic substitution.[9] Although protonated functional groups are more common for lower pH levels, it is plausible that H-bonding only becomes the dominant force upon pH values between 4 and 8 because of the conformational changes that occur in the collagen structure during neutralization. Those modifications are associated with the collagen

self-assembly mechanism and have been studied by Jiang *et al*.,[37] who reported that at low pH, collagen molecules assemble into globular particles that start to extend when the pH reached 4.5 and only assembled into fibrillar structures at a pH higher than 5.5. Collagen fibril formation was confirmed by the UV-Vis spectra of collagen solutions at different pH levels (see Figure 3d). Predictably, for the lower pH values (2 and 4), it was possible to identify the two characteristic collagen absorbance peaks at 220 nm (maximum at 200 nm – not seen) related with the presence of peptide bonds and at 275 nm due to aromatic side chains (tyrosine and phenylalanine).[38, 39] However, with increasing pH, the peak associated with the aromatic residues gradually became a broad shoulder because of the light scattering originating from the aggregation of collagen molecules during fibrillogenesis.[40] Figure 3e shows the variation in size of collagen molecules and GO sheets with increasing pH. It is noticeable that the collagen particle size increased by neutralizing the medium until gelling at approximately pH 8 (it was not possible to measure the size of the collagen fibrils at pH = 8 because of spontaneous hydrogel formation). This variation is likely to be only related to the fibril length increasing since the fibril diameter decreases with increasing pH.[41] Therefore, due to this enlargement of the collagen polymer chain, there will be more sites to increase the H-bonding with the GO sheets and therefore less collagen % will be needed to induce gelation (see Figure S1 in Supporting Information). With regard to GO, the sheets are larger than collagen fibrils and only slight variations in their size can be detected since in acidic medium GO sheets have a predominantly flat arrangement and their conformational changes are mainly related to hydrophilicity dissimilarity between the edge and the basal plane, which increases with the pH.[42] A possible explanation for the marginal decrease in GO sheet size observed at pH = 8 was given by Whitby *et al*.,[43] who concluded that GO sheets usually start to bend and fold at pH > 7 in order to

maximize distance between deprotonated sites and diminish exposure of the basal plane to the aqueous environment (hydrophobic effect).

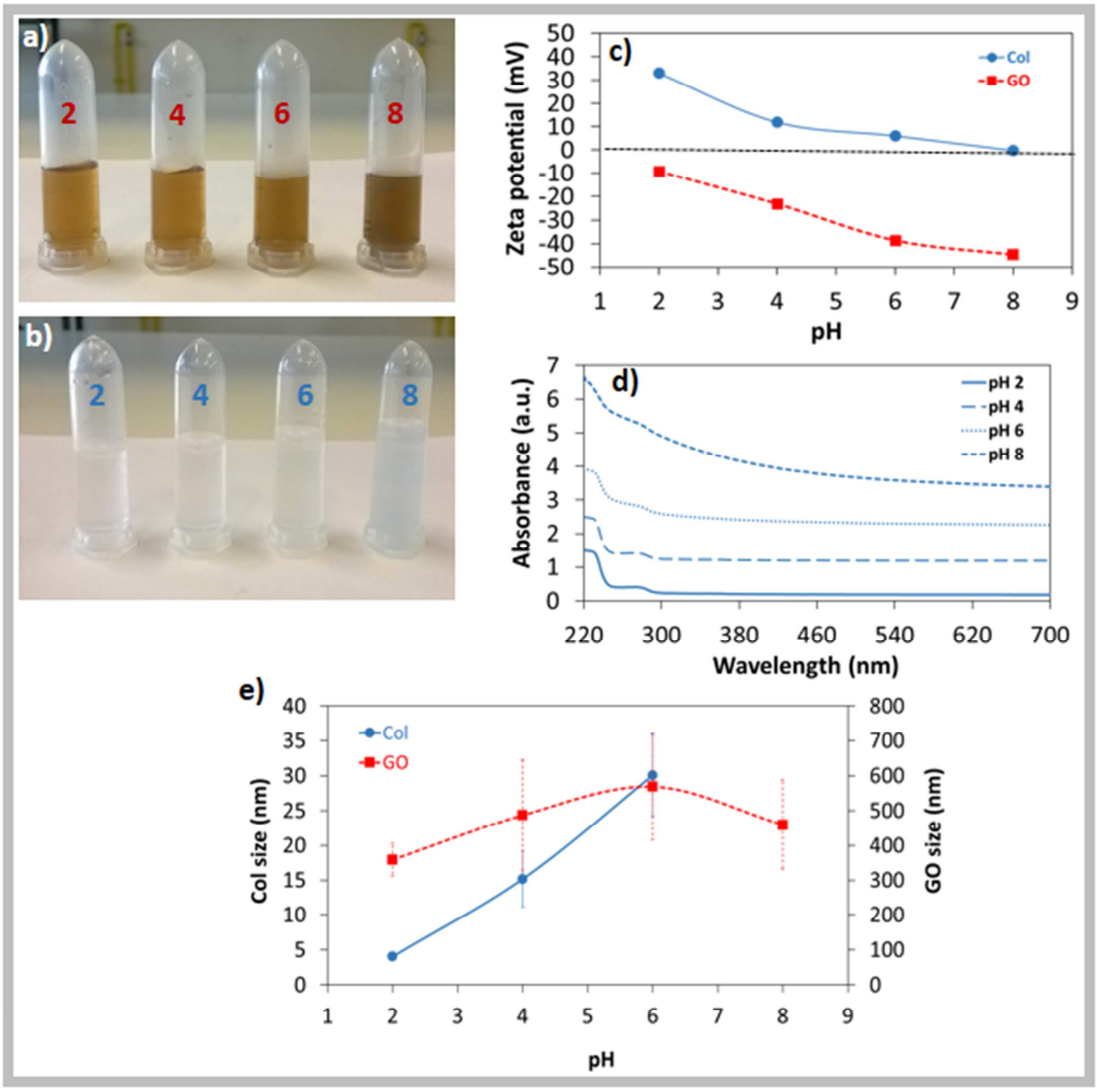

Figure 2. Photographs of **a)** GO and **b)** collagen solutions at different pH levels; **c)** Variation of Zeta potential of collagen and GO with the pH of the aqueous solution; **d)** UV-Vis spectra of collagen aqueous solutions at different pH levels; **e)** Size distribution of the GO and collagen particles in aqueous solution at various pH values;

The strength of the interactions between GO and collagen was further investigated via detailed AFM studies in friction mode. The graphics inserted in Figure 3 showed the linear response of each individual component and the respective hydrogel by applying

four different normal forces: 18.7, 37.3, 74.6 and 149.2 nN, that can be represented by the equation $F_{fr}=K_{fri}(F_{adh} + N)$.[44] The results obtained presented very distinct values of friction coefficients (K_{fri}) for collagen (0.02), GO (0.22) and GO-Col (0.13). Indeed, collagen showed the lower K_{fri} value, which can be attributed to the denatured amorphous fibrillary structure. Contrarily, GO showed the highest K_{fri} characteristic of its oxygenated 2D carbon macromolecular structure that reduces the out-of-plane flexibility of graphene.[45] The GO-Col nanocomposite exhibited an intermediate value for K_{fri} (0.13), which is much higher than denatured collagen fibrils and similar to values observed for natural cartilage tissue.[46] These results strongly suggests that GO surface is able to promote the structural arrangement of collagen fibrils through the establishment of strong interactions, as already predicted by molecular dynamics simulations.[47]

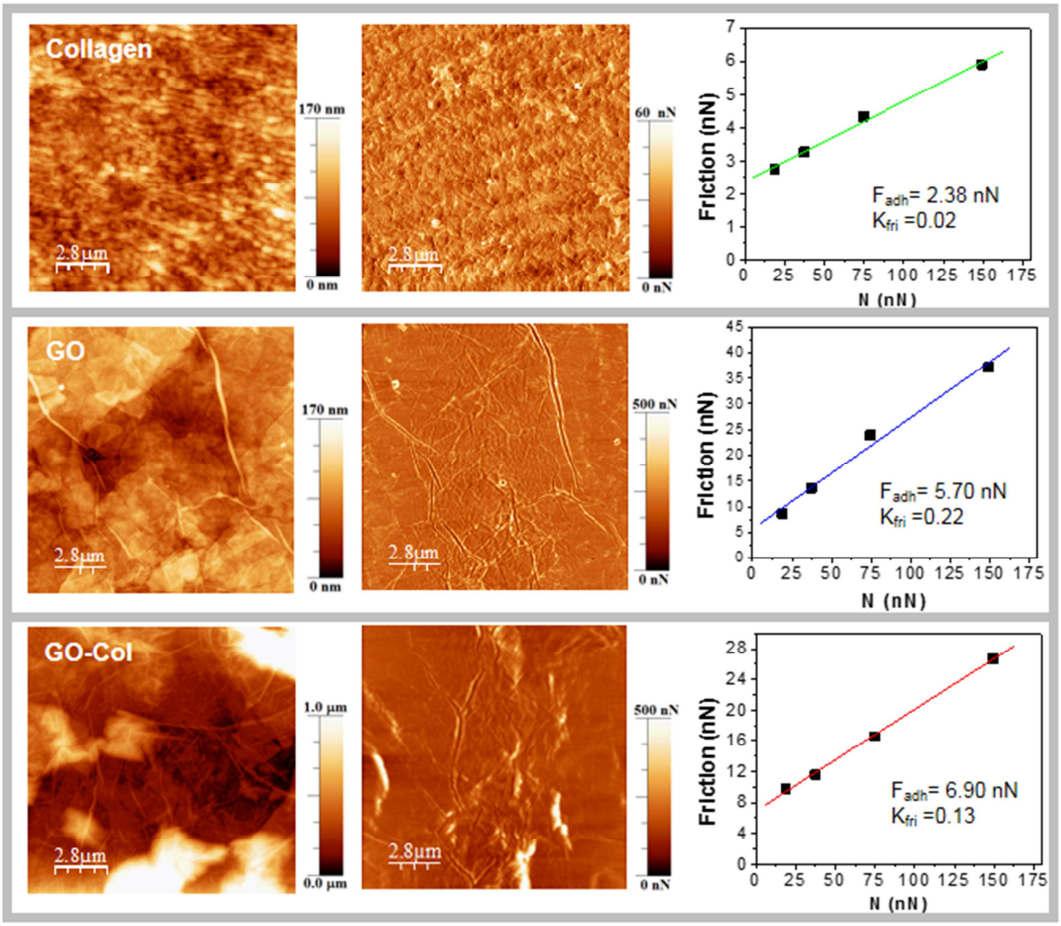

Figure 3. AFM topography and friction (normal force 75 nN) images of collagen fibrils, GO nanosheets and GO-col scaffold. Frictional versus load curves over four load increments for determination of friction coefficient (K_{fri}) and adhesion force (F_{adh}) of different materials.

Characterization of the GO-Col scaffolds

As previously mentioned, the most viable hydrogels, the ones that showed the more uniform shape, were freeze-dried to prepare GO-Col scaffolds. Then, the mechanical integrity was evaluated by swelling and compression tests. This group of scaffolds did not include the 4.12 and 6.6 samples since those proved to be unable to maintain their structure during the washing step. As presented in Table 1 and also shown in Fig. S3 of the Supporting Information, the swelling equilibrium was achieved within 1 hour and

the water uptake capacity of the GO-Col scaffolds was dependent on both the collagen/GO weight ratio and the pH used during the hydrogel synthesis. In fact, for the same pH value, increasing the collagen content in the system caused a reduction in electrostatic repulsion among GO sheets, creating contraction in the hydrogel network and consequently a decrease in the swelling ratio. Additionally, for pH levels where the collagen molecules are larger and can present a fibrillar conformation (4 and 6), increasing the crosslinking agent should result in more H-bonding between their amine and hydroxyl groups and the oxygen containing groups on GO. This would consequently lead to a smaller number of accessible functional groups on the GO-Col network available to establish H-bonds with water molecules during the swelling process. Conversely, water uptake tends to increase with increasing pH, for the same collagen amount, since during hydrogel preparation the continuous deprotonation of functional groups intensifies repulsion forces between GO sheets and causes an expansion in the hydrogel network.

The compressive properties of the GO-Col scaffolds were investigated by analysing their typical stress-strain curves (see Figures S4, S5 and S6 in Supporting Information). It was observed that during the compressive tests, independently of the pH and % collagen used during hydrogel synthesis, scaffolds in different states (dry and wet) did not fracture at the stress levels applied (max. 5 MPa). This revealed an efficient degree of crosslinking between GO and collagen due to successful interconnection of their individual networks. The compressive moduli of the scaffolds exhibited similar variations in both dry and wet states, depending on the pH of the medium and the % of collagen (see Table 1 and Figure S7 in Supporting Information). In fact, as the increasing pH caused the availability of new crosslinking sites on the collagen chain during fibril formation (pH 4 and 6), there was more H-bonding between collagen and

GO sheets and therefore a gradual increase in compressive modulus due a more compact hydrogel network. Similarly, the compressive modulus increased with the addition of collagen into the system because of the subsequent decrease in electrostatic repulsion among GO sheets, which initiates the contraction of the GO-Col network. The differences between the compressive moduli of dry and wet scaffolds are deeply related to the swelling response discussed above. Indeed, as water molecules can readily interact with free hydrophilic groups of both GO and collagen and weaken the already established intermolecular H-bonds,[48] the decline of the scaffold structural integrity will increase for higher swelling ratios.

Table 1. Summary of the swelling and compressive results obtained for the GO-Col scaffolds.

Scaffold	**Swelling ratio (1h)**	**Swelling ratio (24h)**	**Compressive modulus in a dry state (kPa)**	**Compressive modulus in a wet state (kPa)**
2.18	52.93 ± 2.68	54.52 ± 5.78	12.58 ± 0.55	4.83 ± 0.46
2.24	43.45 ± 2.89	44.23 ± 4.00	15.75 ± 0.64	6.40 ± 0.56
4.18	63.65 ± 6.67	63.98 ± 5.18	15.20 ± 1.84	3.13 ± 0.35
4.24	50.41 ± 7.26	50.13 ± 2.96	17.70 ± 0.64	5.95 ± 1.06
6.12	72.75 ± 8.28	70.60 ± 10.07	17.52 ± 1.44	4.03 ± 0.57

Based on these results, the scaffold 2.24 was selected as the best GO-Col scaffold composition to take forward, since its structural integrity appeared to be the most resistant to water uptake. It showed the lowest swelling ratio and, consequently, the higher compressive modulus in the wet state. In fact, the 2.24 GO-Col scaffold allows the formation of a very compact GO-Col network due to the low pH level used during its preparation and the % of collagen present. In addition to this, the higher percentage

of collagen (relative to 2.18) should theoretically enhance the biocompatibility of the scaffold during cell culture procedures. Hereafter the 2.24 GO-Col scaffold will be referred to as GO-Col.

Structural evaluation of optimized GO-Col scaffold and its reduced counterpart

In addition to the biocompatibility and favourable cell responses reported previously,[49] GO and rGO based scaffolds present dissimilar physicochemical properties[50] that can be used to modulate cell adhesion, proliferation and differentiation. Indeed, by removing oxygen containing groups from the GO surface during the reduction process, features like the conductivity[51] and hydrophilicity (which influences the interactions between material surface and proteins in the culture medium[52, 53]) will change, potentially modulating cell behaviour.[11]

The reduction process of the GO-Col scaffold was firstly indicated by a color change from brown (see Figure 4a) to black (see Figure 4b) after the hydrazine treatment. SEM analysis of both GO-Col and rGO-Col scaffolds showed heterogeneous microporous structures with pore size distributions between 20 μm to 100 μm. We hypothesize that the observed alveolar pore shape occurs due to the preferential self-assembly of the GO sheets by the edges since that regions are highly electronegative due to the high density of carboxylic groups, favoring the ionic interaction with the electropositive amine groups of collagen during GO-Col hydrogel formation.

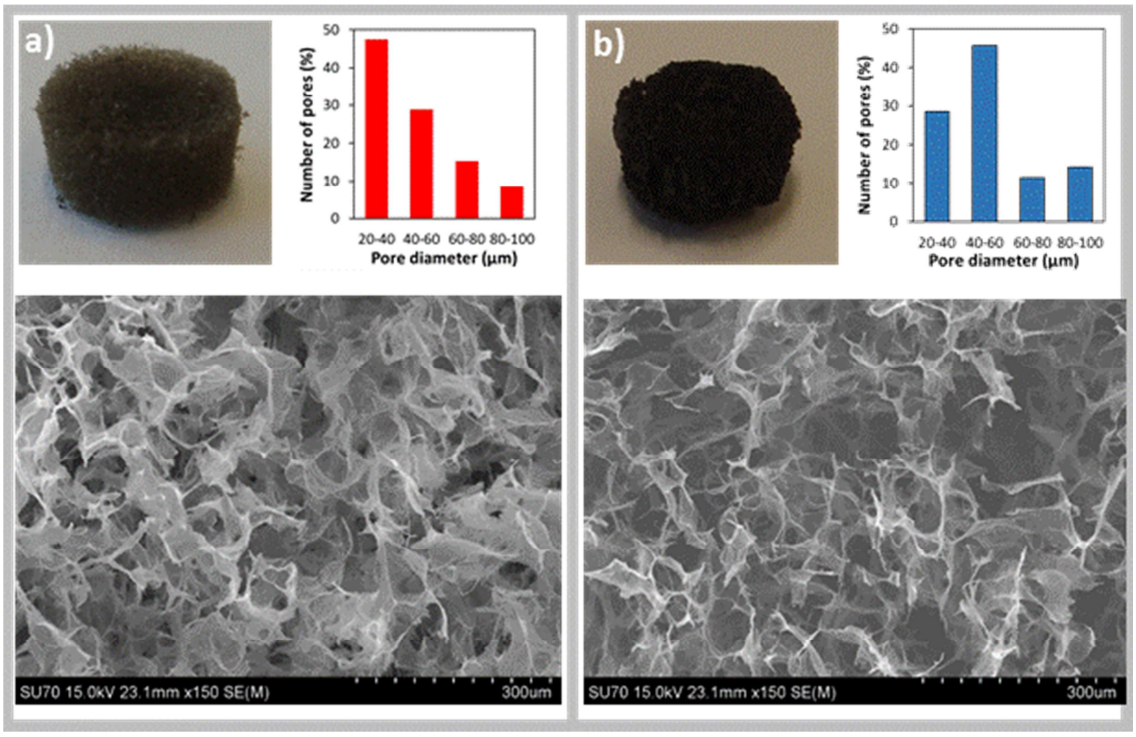

Figure 4. Microporous architecture of **a)** the GO-Col and **b)** rGO-Col scaffolds, showing in both cases a photograph of the scaffold, the correspondent SEM microstructure and the pore size distribution.

These two scaffolds were analysed by ATR-FTIR (see Figure 5a). As expected, the GO-Col spectrum displayed characteristic bands of both GO[54] and collagen.[55] Indeed, the strong peak located at 1640 cm^{-1} is not only related to the C=C and C=O (carbonyl) stretching vibrations of the GO portion, but also to the C=O stretching of the amide I in the collagen chain. Likewise, the band situated at 1240 cm^{-1} is probably due to the contribution of the stretching vibration of epoxy groups on the GO surface and the N-H bending coupled with C-N stretching of the amide III located in the collagen structure. The other absorbance bands related with GO oxygen functionalities are located at 985 cm^{-1} (epoxy), 1049 cm^{-1} (alkoxy), 1740 cm^{-1} (carboxyl) and 3350 cm^{-1} (hydroxyl). Finally, it is also possible to observe an absorbance band related with the amide II of collagen at 1555 cm^{-1}. After reduction (rGO-Col spectrum), there were changes in the

absorbance patterns of the oxygen functionalities translated in an overall reduction of the intensity of the bands correspondents of oxygen functional groups, with less impact on most resilient functional groups such as carboxylic acids (1740 cm^{-1}), alkoxy (1049 cm^{-1}) and high impact on the most instable ones such as hydroxyl (3350 cm^{-1}) and epoxy (985 cm^{-1}).

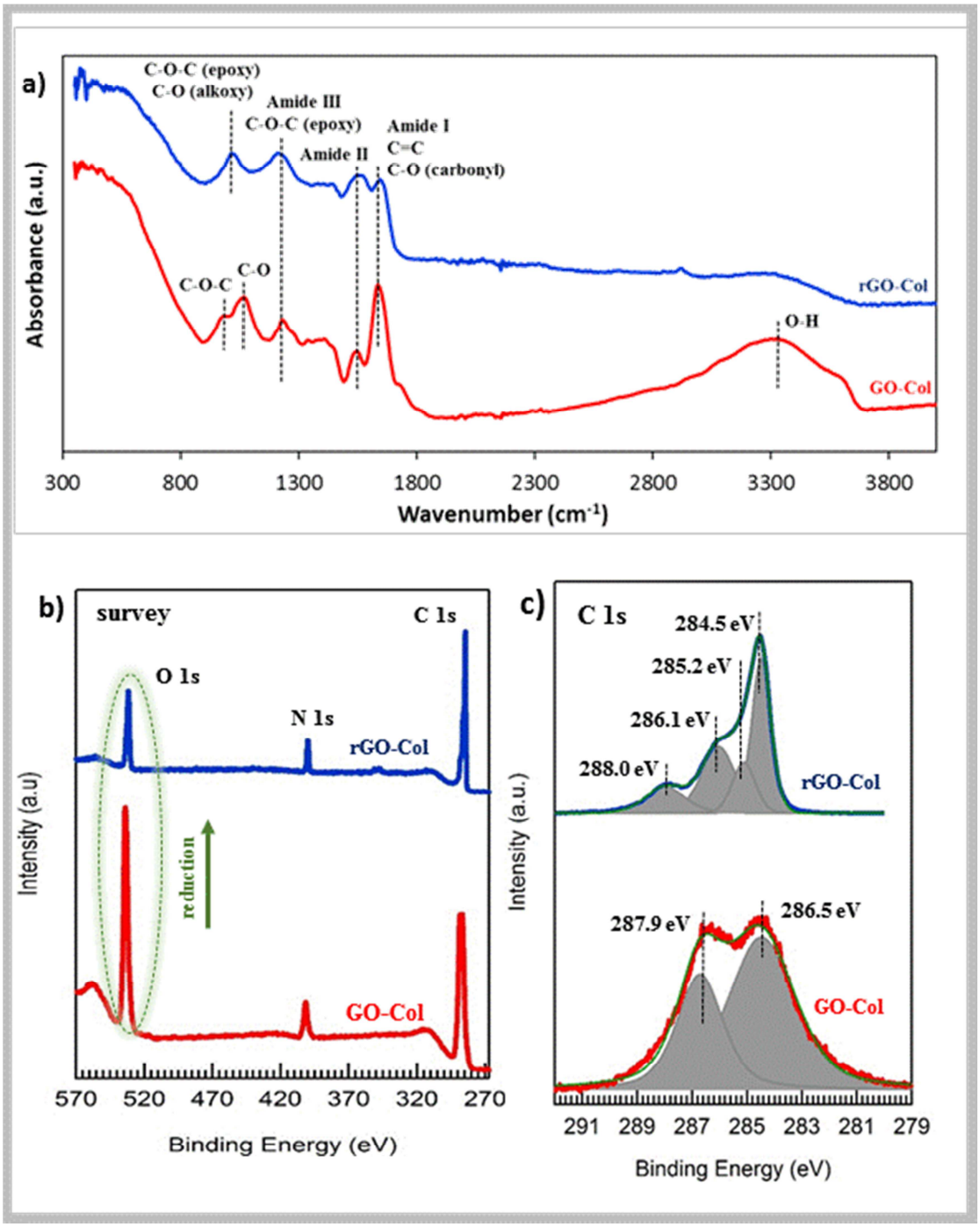

Figure 5. Chemical characterization of the GO-Col and rGO-Col scaffolds. a) ATR-FTIR; b-c) XPS characterization: b) wide scans and c) high resolution C1s core level. The best fits are also included and the spectra were normalized for direct comparison.

Wide-scan XPS survey spectra were also recorded for the GO-Col and rGO-Col scaffolds (see Figure 5b). The direct comparison between both O 1s core levels clearly indicates a strong reduction of the oxygen species on the rGO-Col scaffold (see Table S2 in Supporting Information). Importantly, the reduction of the sample is clear by comparing the ratio of the areas of the C1s and O1s core levels in the wide scans. In the case of GO-Col sample the C1s/O1s ratio is 2.4 while in its reduced form is 5.0, indicating that oxygen species leave the sample as expected during the reduction process[6]. On the contrary, the ratio between the areas of the C1s and N1s does not change during the reduction of the sample. The value obtained in both cases for C1s/N1s is close to 10, indicating that no degradation of collagen during the hydrazine treatment under the experimental conditions used.[56]

As shown in Figure 5c, C 1s core level spectra recorded for rGO-Col sample shows 4 main features which were assigned to C sp^2 (~284.5eV), C sp^3/C-N (~285.2eV), C-O (~286.1 eV) and C=O (~288.0eV), on the other hand, its oxygenated contra-part showed a lower resolution spectrum since only 2 main features were assigned to C sp^2 / C sp^3/ C-N (~284.5eV) and C-O / C=O (~286.7 eV). In this figure the intensity of the spectra was normalized to allow direct comparison between the scaffolds. The binding energy shifts observed could be related to surface charge effects of the non-conductive sample.[57]

Furthermore, we confirmed the removal of the oxygen containing groups and the rearrangement of the carbon atoms into a sp^2 configuration by measuring the increasing conductance of the GO-Col scaffold after the reduction process[58]. The difference

between the conductance of the GO-Col scaffold (0.125 μS) and the rGO-Col scaffold (142 μS) was of three orders of magnitude.

The result of the swelling response of these two scaffolds is summarized in Table 2 and in Figure S8a of the Supporting Information. It is possible to observe that after the reduction process and independently of the swelling period tested (1 h and 24 h), there was a remarkable increase in the water uptake capacity of the r-GO scaffold regardless of its expected hydrophobic nature due to the oxygen groups removal, when compared with the GO-Col. This was probably due to the maintenance of the interconnected microporous network after the reduction process. To mention that the fewer amounts of hydrophilic groups on the rGO sheets of the rGO-Col scaffolds (high C/O ratio) most probably helped to prevent the interaction between water molecules and the rGO-Col network, which consequently minimized damage to the structure during swelling, allowing the entrance of more water molecules. As reported by Xie *et al.*,[59] the wettability of freeze-dried graphene sponges can be modulated by controlling the pore size of the structure, which can be water absorbent if its pores are smaller than 250 μm, being this statement valid for both scaffolds.

Table 2. Summary of the swelling and compressive results obtained for the GO-Col and rGO-Col scaffolds.

Scaffold	**Swelling ratio (1h)**	**Swelling ratio (24h)**	**Compressive modulus in a dry state (kPa)**	**Compressive modulus in a wet state (kPa)**
GO-Col	43.45 ± 2.89	44.23 ± 4.00	15.75 ± 0.64	6.40 ± 0.56
rGO-Col	91.27 ± 11.51	92.63 ± 14.51	15.25 ± 1.62	12.80 ± 1.27

The compressive properties of these scaffolds were also compared (see Table 2 and Figure S8b in Supporting Information). Although, in the dry state the mechanical

behaviour is similar for the reduced and the non-reduced forms; in the wet state the compressive modulus of GO-Col is reduced by approximately 60 %. Interestingly, the rGO-Col presents a compressive modulus reduction of only 16 %. This result is a direct consequence of the resistance of the rGO-Col scaffold to water damage because of its higher C/O ratio, which weaken the formation of H-bonds between the scaffold and the water molecules as discussed previously. Indeed, the water uptake did not cause any relevant structural damage to the rGO-Col scaffold.

Envisaging the application of these scaffolds in tissue engineering, its important to investigate their potentiality to integrate strategies that include dynamic mechanical stimulation, which has been an approach increasingly used in applications including the modulation of stem cells behavior.[60, 61] In this context, the scaffolds were subjected to fatigue tests. Figure 6a shows a photograph of the dynamic compression system apparatus. The graphical representation in Figure 6b, where the stress amplitude applied to the scaffolds is plotted against the number of cycles, show that both scaffolds are skilled of withstand during a significant period of time, which frequency (0.2Hz) and deformation (5%) are compatible with dynamic cell culture assays.[62-64]

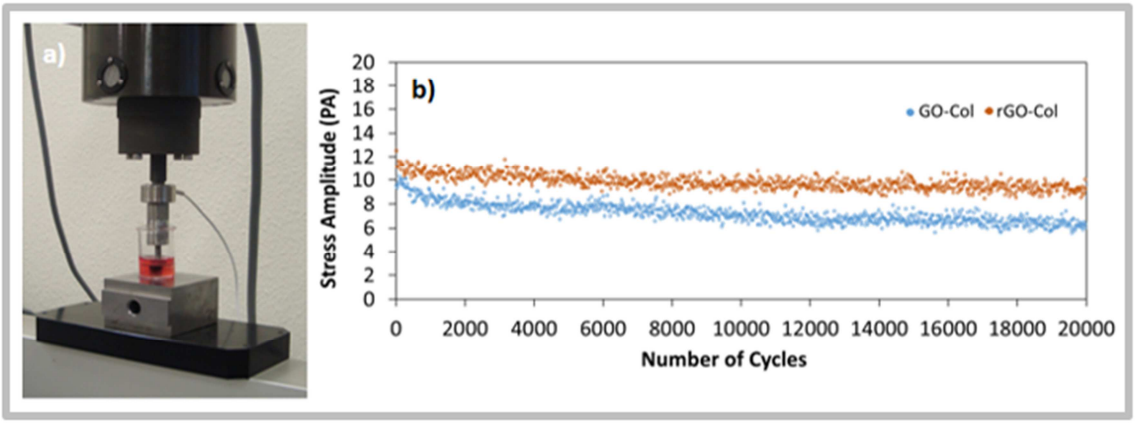

Figure 6. Comparison of the mechanical response of the GO-Col and rGO-Col scaffolds under dynamic compression cycles. a) Dynamic compression system

apparatus; b) Stress amplitude versus number of cycles curves of the GO-Col scaffold (blue) and its reduced counterpart (orange)

Cytocompatibility of GO-Col and rGO-Col scaffolds

To obtain a first insight about the potential of both GO-Col and rGO-Col scaffolds for biomimetic cellular microenvironment, we made some preliminary tests about the viability of Schwann cells cultured on these materials surfaces. As seen in Figure 7a, there was no difference between the numbers of cultured cells on both scaffolds after 24 h of incubation.

Fluorescence microscopy images (see Figures 7b and 7c) are in agreement with the high-resolution SEM images (see Figures 7d and 7e) and show that the cells spread extensively on both materials and formed attachments to the surface via pseudopods such as filopodia. These results show that the GO-Col and its reduced counterpart are able to support living Schwann cells and promote cell spreading. It appears that the fewer oxygen groups on the rGO surface did not interfere with the ability of the scaffold to successfully interact with cells. This could be explained by the presence of cellular anchor sites provided via the π-π interactions that the rGO can establish with the inner hydrophobic core of medium proteins[15] and via the oxygen moieties that have resisted the reduction process.

Further studies should evaluate the effects of the dissimilar chemical composition of the GO-Col and rGO-Col scaffolds on the adsorption capacity of medium proteins and on the type of surface-biomolecule interaction established since these factors may influence several aspects of cell behaviour.[12, 15]

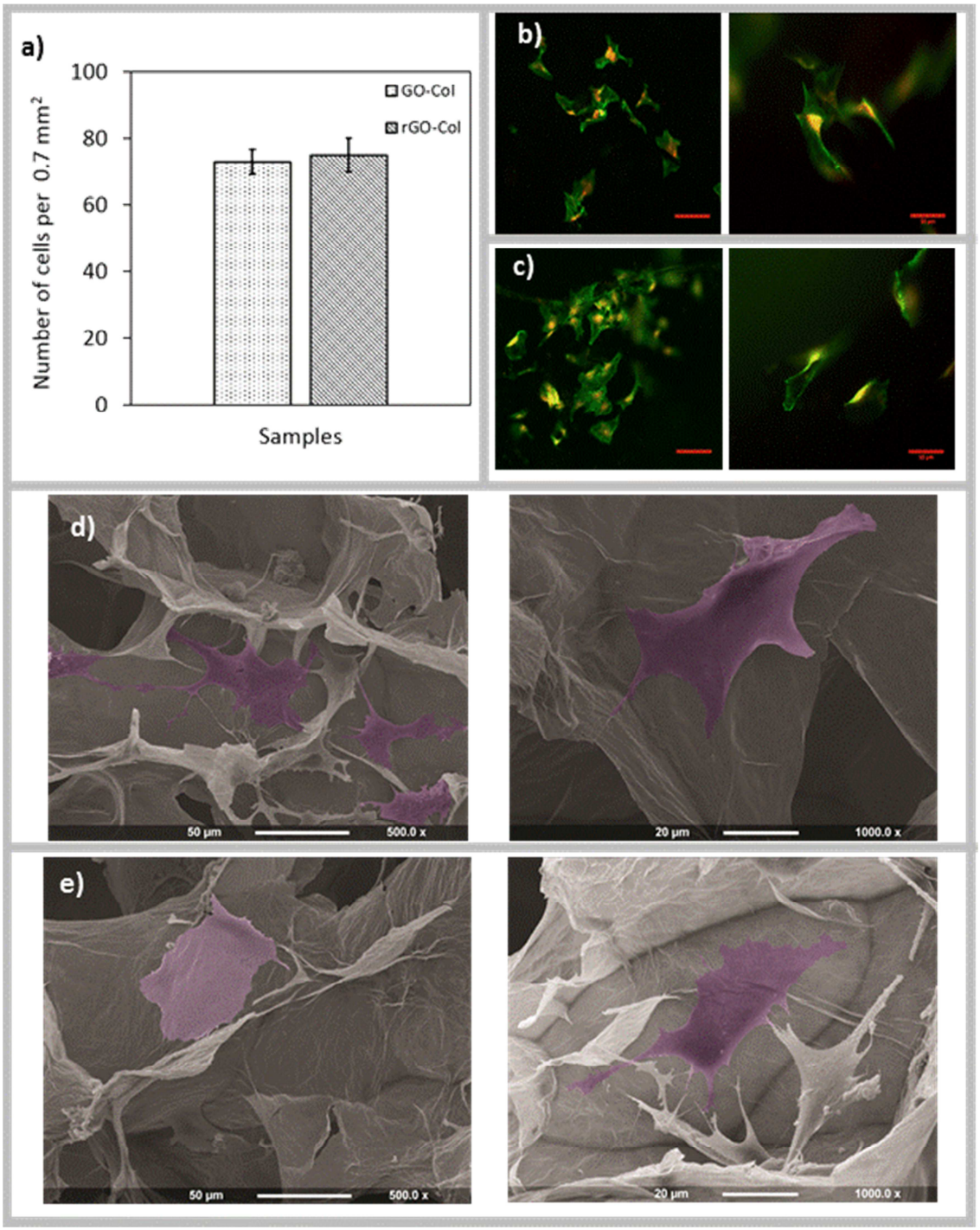

Figure 7. a) Viability of Schwann cells on GO-Col and rGO-Col scaffolds following 24h incubation. Live cells were distinguished from dead cells and the number of live cells per area was determined. One-way ANOVA revealed no statistical significance between test samples. Data are means ± SEM, n=3; b-c) Micrographs showing Schwann cells seeded on GO-Col scaffolds (b) and rGO-Col scaffolds (c) after 24h in culture at a magnification of 10x (left - scale bar = 100 µm) and 20x (right - scale bar = 50 µm). The

staining markers are F-actin (green) and Propidium iodide (red); d-e) SEM images showing cell-material interactions for GO-Col (d) scaffolds and rGO-Col (e) scaffolds. Schwann cells are coloured in purple.

4. Conclusions

In the present study, collagen was used as a crosslinker for GO nanosheets in acidic medium to prepare a portfolio of self-assembled GO-Col hydrogels with mechanical and swelling properties that were dependent on the medium pH and on the amount of collagen used during the gelation process. Due to a systematic characterization study we were able to confirm and characterize in detail the electrostatic nature of the bonds between the protonated amine groups from collagen and the anionic carboxylic groups from GO. We also identified the GO-Col hydrogel produced at a pH value 2 and with a 24% Col/GO w/w ratio as the most appropriate candidate to be explored as a scaffold for future biological testing. Additionally, the GO-Col scaffold was reduced and its mechanical integrity evaluated, showing a much greater structural integrity in the wet state when compared with its oxidized counterpart. Both GO-Col and rGO-Col scaffolds showed suitable cell-material interactions with Schwann cells and consequently an appreciable potential for use in mechanically stimulated cellular environments for future tissue engineering applications.

Acknowledgements

PAAP Marques thank the Portuguese Foundation for Science and Technology (FCT) for the investigator grant (IF/00917/2013) and for the project

IF/00917/2013/CP1162/CT0016 which supports the researcher grant of André Girão.

Gil Gonçalves and Gonzalo Otero also thank FCT for respectively the grants SFRH/BDP/84419/2012 and SFRH/BPD/90562/2012. Manoj Singh acknowledges FCT for his 2013 FCT Investigator programme.

This work was supported by the National Institute for Health Research (NIHR) University College London Hospitals (UCLH) Biomedical Research Centre (BRC) and the UCL Doctoral Training Programme in Medical Devices.

References

1. Zhang, H.; Gruner, G.; Zhao, Y. Recent advancements of graphene in biomedicine. *Journal of Materials Chemistry B* **2013**, 1, 2542-2567.
2. Avouris, P. Graphene: Electronic and Photonic Properties and Devices. *Nano Letters* **2010**, 10, 4285-4294.
3. Cong, H.-P.; Chen, J.-F.; Yu, S.-H. Graphene-based macroscopic assemblies and architectures: an emerging material system. *Chemical Society Reviews* **2014**, 43, 7295-7325.
4. Zhang, Y.; Zhang, L.; Zhou, C. Review of Chemical Vapor Deposition of Graphene and Related Applications. *Accounts of Chemical Research* **2013**, 46, 2329-2339.
5. Chua, C. K.; Pumera, M. Chemical reduction of graphene oxide: a synthetic chemistry viewpoint. *Chemical Society Reviews* **2014**, 43, 291-312.
6. Dreyer, D. R.; Park, S.; Bielawski, C. W.; Ruoff, R. S. The chemistry of graphene oxide. *Chemical Society Reviews* **2010**, 39, 228-240.
7. Pei, S.; Cheng, H.-M. The reduction of graphene oxide. *Carbon* **2012**, 50, 3210-3228.
8. Goenka, S.; Sant, V.; Sant, S. Graphene-based nanomaterials for drug delivery and tissue engineering. *Journal of Controlled Release* **2014**, 173, 75-88.
9. Liu, J.; Cui, L.; Losic, D. Graphene and graphene oxide as new nanocarriers for drug delivery applications. *Acta Biomaterialia* **2013**, 9, 9243-9257.
10. Marques, P. A. A. P.; Gonçalves, G.; Cruz, S.; Almeida, N.; Singh, M. K.; Grácio, J.; Suosa, A. C. M. *Functionalized Graphene Nanocomposites*. **2011**.
11. Ku, S. H.; Park, C. B. Myoblast differentiation on graphene oxide. *Biomaterials* **2013**, 34, 2017-2023.
12. Chen, G. Y.; Pang, D. W. P.; Hwang, S. M.; Tuan, H. Y.; Hu, Y. C. A graphene-based platform for induced pluripotent stem cells culture and differentiation. *Biomaterials* **2012**, 33, 418-427.
13. Bressan, E.; Ferroni, L.; Gardin, C.; Sbricoli, L.; Gobbato, L.; Ludovichetti, F. S.; Tocco, I.; Carraro, A.; Piattelli, A.; Zavan, B. Graphene based scaffolds effects on stem cells commitment. *J Transl Med* **2014**, 12, 296.
14. Ruiz, O. N.; Fernando, K. A. S.; Wang, B.; Brown, N. A.; Luo, P. G.; McNamara, N. D.; Vangsness, M.; Sun, Y.-P.; Bunker, C. E. Graphene Oxide: A Nonspecific Enhancer of Cellular Growth. *ACS Nano* **2011**, 5, 8100-8107.
15. Lee, W. C.; Lim, C. H. Y. X.; Shi, H.; Tang, L. A. L.; Wang, Y.; Lim, C. T.; Loh, K. P. Origin of Enhanced Stem Cell Growth and Differentiation on Graphene and Graphene Oxide. *ACS Nano* **2011**, 5, 7334-7341.
16. Qi, W.; Yuan, W.; Yan, J.; Wang, H. Growth and accelerated differentiation of mesenchymal stem cells on graphene oxide/poly-l-lysine composite films. *Journal of Materials Chemistry B* **2014**, 2, 5461-5467.
17. Sayyar, S.; Murray, E.; Thompson, B. C.; Gambhir, S.; Officer, D. L.; Wallace, G. G. Covalently linked biocompatible graphene/polycaprolactone composites for tissue engineering. *Carbon* **2013**, 52, 296-304.
18. Wang, X.; Bai, H.; Yao, Z.; Liu, A.; Shi, G. Electrically conductive and mechanically strong biomimetic chitosan/reduced graphene oxide composite films. *Journal of Materials Chemistry* **2010**, 20, 9032-9036.
19. Qi, Y. Y.; Tai, Z. X.; Sun, D. F.; Chen, J. T.; Ma, H. B.; Yan, X. B.; Liu, B.; Xue, Q. J. Fabrication and characterization of poly(vinyl alcohol)/graphene oxide nanofibrous biocomposite scaffolds. *Journal of Applied Polymer Science* **2013**, 127, 1885-1894.

20. Jagur-Grodzinski, J. Polymeric gels and hydrogels for biomedical and pharmaceutical applications. *Polymers for Advanced Technologies* **2010**, 21, 27-47.
21. Bai, H.; Sheng, K.; Zhang, P.; Li, C.; Shi, G. Graphene oxide/conducting polymer composite hydrogels. *Journal of Materials Chemistry* **2011**, 21, 18653-18658.
22. Bai, H.; Li, C.; Wang, X.; Shi, G. A pH-sensitive graphene oxide composite hydrogel. *Chemical Communications* **2010**, 46, 2376-2378.
23. Piao, Y.; Chen, B. Self-assembled graphene oxide–gelatin nanocomposite hydrogels: Characterization, formation mechanisms, and pH-sensitive drug release behavior. *Journal of Polymer Science Part B: Polymer Physics* **2015**, 53, 356-367.
24. Huang, C.; Bai, H.; Li, C.; Shi, G. A graphene oxide/hemoglobin composite hydrogel for enzymatic catalysis in organic solvents. *Chemical Communications* **2011**, 47, 4962-4964.
25. Chen, Y.; Chen, L.; Bai, H.; Li, L. Graphene oxide-chitosan composite hydrogels as broad-spectrum adsorbents for water purification. *Journal of Materials Chemistry A* **2013**, 1, 1992-2001.
26. Abou Neel, E. A.; Bozec, L.; Knowles, J. C.; Syed, O.; Mudera, V.; Day, R.; Hyun, J. K. Collagen--emerging collagen based therapies hit the patient. *Adv Drug Deliv Rev* **2013**, 65, 429-56.
27. Abou Neel, E. A.; Cheema, U.; Knowles, J. C.; Brown, R. A.; Nazhat, S. N. Use of multiple unconfined compression for control of collagen gel scaffold density and mechanical properties. *Soft Matter* **2006**, 2, 986-992.
28. Deepachitra, R.; Ramnath, V.; Sastry, T. P. Graphene oxide incorporated collagen-fibrin biofilm as a wound dressing material. *RSC Advances* **2014**, 4, 62717-62727.
29. Shin, Y.; Lee, J.; Jin, L.; Kim, M.; Kim, Y.-J.; Hyun, J.; Jung, T.-G.; Hong, S.; Han, D.-W. Stimulated myoblast differentiation on graphene oxide-impregnated PLGA-collagen hybrid fibre matrices. *Journal of Nanobiotechnology* **2015**, 13, 21.
30. Kang, S.; Park, J. B.; Lee, T.-J.; Ryu, S.; Bhang, S. H.; La, W.-G.; Noh, M.-K.; Hong, B. H.; Kim, B.-S. Covalent conjugation of mechanically stiff graphene oxide flakes to three-dimensional collagen scaffolds for osteogenic differentiation of human mesenchymal stem cells. *Carbon* **2015**, 83, 162-172.
31. Kanayama, I.; Miyaji, H.; Takita, H.; Nishida, E.; Tsuji, M.; Fugetsu, B.; Sun, L.; Inoue, K.; Ibara, A.; Akasaka, T.; Sugaya, T.; Kawanami, M. Comparative study of bioactivity of collagen scaffolds coated with graphene oxide and reduced graphene oxide. *Int J Nanomedicine* **2014**, 9, 3363-73.
32. Bai, H.; Li, C.; Wang, X.; Shi, G. On the Gelation of Graphene Oxide. *The Journal of Physical Chemistry C* **2011**, 115, 5545-5551.
33. Sahu, A.; Choi, W. I.; Tae, G. A stimuli-sensitive injectable graphene oxide composite hydrogel. *Chem Commun (Camb)* **2012**, 48, 5820-2.
34. Jaiswal, M. K.; Xavier, J. R.; Carrow, J. K.; Desai, P.; Alge, D.; Gaharwar, A. K. Mechanically Stiff Nanocomposite Hydrogels at Ultralow Nanoparticle Content. *ACS Nano* **2016**, 10, 246-256.
35. Spyrou, K.; Potsi, G.; Diamanti, E. K.; Ke, X.; Serestatidou, E.; Verginadis, I. I.; Velalopoulou, A. P.; Evangelou, A. M.; Deligiannakis, Y.; Van Tendeloo, G.; Gournis, D.; Rudolf, P. Towards Novel Multifunctional Pillared Nanostructures: Effective Intercalation of Adamantylamine in Graphene Oxide and Smectite Clays. *Advanced Functional Materials* **2014**, 24, 5841-5850.
36. Goncalves, G.; Marques, P. A. A. P.; Granadeiro, C. M.; Nogueira, H. I. S.; Singh, M. K.; Grácio, J. Surface Modification of Graphene Nanosheets with Gold Nanoparticles: The Role of Oxygen Moieties at Graphene Surface on Gold Nucleation and Growth. *Chemistry of Materials* **2009**, 21, 4796-4802.
37. Jiang, F.; Horber, H.; Howard, J.; Muller, D. J. Assembly of collagen into microribbons: effects of pH and electrolytes. *J Struct Biol* **2004**, 148, 268-78.

38. Metreveli, N. O.; Jariashvili, K. K.; Namicheishvili, L. O.; Svintradze, D. V.; Chikvaidze, E. N.; Sionkowska, A.; Skopinska, J. UV-vis and FT-IR spectra of ultraviolet irradiated collagen in the presence of antioxidant ascorbic acid. *Ecotoxicol Environ Saf* **2010**, 73, 448-55.
39. Vincentelli, R.; Canaan, S.; Campanacci, V.; Valencia, C.; Maurin, D.; Frassinetti, F.; Scappucini-Calvo, L.; Bourne, Y.; Cambillau, C.; Bignon, C. High-throughput automated refolding screening of inclusion bodies. *Protein Sci* **2004**, 13, 2782-92.
40. Li, Y.; Asadi, A.; Monroe, M. R.; Douglas, E. P. pH effects on collagen fibrillogenesis in vitro: Electrostatic interactions and phosphate binding. *Materials Science and Engineering: C* **2009**, 29, 1643-1649.
41. Achilli, M.; Mantovani, D. Tailoring Mechanical Properties of Collagen-Based Scaffolds for Vascular Tissue Engineering: The Effects of pH, Temperature and Ionic Strength on Gelation. *Polymers* **2010**, 2, 664.
42. Shih, C.-J.; Lin, S.; Sharma, R.; Strano, M. S.; Blankschtein, D. Understanding the pH-Dependent Behavior of Graphene Oxide Aqueous Solutions: A Comparative Experimental and Molecular Dynamics Simulation Study. *Langmuir* **2012**, 28, 235-241.
43. Whitby, R. L. D.; Gun'ko, V. M.; Korobeinyk, A.; Busquets, R.; Cundy, A. B.; László, K.; Skubiszewska-Zięba, J.; Leboda, R.; Tombácz, E.; Toth, I. Y.; Kovacs, K.; Mikhalovsky, S. V. Driving Forces of Conformational Changes in Single-Layer Graphene Oxide. *ACS Nano* **2012**, 6, 3967-3973.
44. Foster, T. T.; Alexander, M. R.; Leggett, G. J.; McAlpine, E. Friction Force Microscopy of Alkylphosphonic Acid and Carboxylic Acids Adsorbed on the Native Oxide of Aluminum. *Langmuir* **2006**, 22, 9254-9259.
45. Berman, D.; Erdemir, A.; Sumant, A. V. Graphene: a new emerging lubricant. *Materials Today* **2014**, 17, 31-42.
46. Park, S.; Costa, K. D.; Ateshian, G. A. Microscale frictional response of bovine articular cartilage from atomic force microscopy. *J Biomech* **2004**, 37, 1679-87.
47. Heidari, H.; Shamloo, A. The effect of rippled graphene sheet roughness on the adhesive characteristics of a collagen–graphene system. *International Journal of Adhesion and Adhesives* **2016**, 64, 9-14.
48. Han, D.; Yan, L.; Chen, W.; Li, W. Preparation of chitosan/graphene oxide composite film with enhanced mechanical strength in the wet state. *Carbohydrate Polymers* **2011**, 83, 653-658.
49. Lee, S. K.; Kim, H.; Shim, B. S. Graphene: an emerging material for biological tissue engineering. *Carbon Lett* **2013**, 14, 63-75.
50. Compton, O. C.; Nguyen, S. T. Graphene Oxide, Highly Reduced Graphene Oxide, and Graphene: Versatile Building Blocks for Carbon-Based Materials. *Small* **2010**, 6, 711-723.
51. Zhang, L. L.; Zhao, X.; Stoller, M. D.; Zhu, Y.; Ji, H.; Murali, S.; Wu, Y.; Perales, S.; Clevenger, B.; Ruoff, R. S. Highly Conductive and Porous Activated Reduced Graphene Oxide Films for High-Power Supercapacitors. *Nano Letters* **2012**, 12, 1806-1812.
52. Zhang, Y.; Zhang, J.; Huang, X.; Zhou, X.; Wu, H.; Guo, S. Assembly of graphene oxide-enzyme conjugates through hydrophobic interaction. *Small* **2012**, 8, 154-9.
53. Gupta, S.; Irihamye, A. Probing the nature of electron transfer in metalloproteins on graphene-family materials as nanobiocatalytic scaffold using electrochemistry. *AIP Advances* **2015**, 5, 037106.
54. Zhou, X.; Zhang, J.; Wu, H.; Yang, H.; Zhang, J.; Guo, S. Reducing Graphene Oxide via Hydroxylamine: A Simple and Efficient Route to Graphene. *The Journal of Physical Chemistry C* **2011**, 115, 11957-11961.
55. Jackson, M.; Choo, L. P.; Watson, P. H.; Halliday, W. C.; Mantsch, H. H. Beware of connective tissue proteins: assignment and implications of collagen absorptions in infrared spectra of human tissues. *Biochim Biophys Acta* **1995**, 1270, 1-6.
56. de la Burde, R.; Peckham, L.; Veis, A. The Action of Hydrazine on Collagen: I. CHEMICAL MODIFICATION. *Journal of Biological Chemistry* **1963**, 238, 189-197.

57. Gao, F.; Wang, Y.; Burkholder, L.; Tysoe, W. T. Chemistry of l-proline on Pd(1 1 1): Temperature-programmed desorption and X-ray photoelectron spectroscopic study. *Surface Science* **2007**, 601, 3579-3588.
58. Gómez-Navarro, C.; Weitz, R. T.; Bittner, A. M.; Scolari, M.; Mews, A.; Burghard, M.; Kern, K. Electronic Transport Properties of Individual Chemically Reduced Graphene Oxide Sheets. *Nano Letters* **2007**, 7, 3499-3503.
59. Xie, X.; Zhou, Y.; Bi, H.; Yin, K.; Wan, S.; Sun, L. Large-range Control of the Microstructures and Properties of Three-dimensional Porous Graphene. *Sci. Rep.* **2013**, 3.
60. Wang, Y. K.; Chen, C. S. Cell adhesion and mechanical stimulation in the regulation of mesenchymal stem cell differentiation. *J Cell Mol Med* **2013**, 17, 823-32.
61. Luu, Y. K.; Capilla, E.; Rosen, C. J.; Gilsanz, V.; Pessin, J. E.; Judex, S.; Rubin, C. T. Mechanical stimulation of mesenchymal stem cell proliferation and differentiation promotes osteogenesis while preventing dietary-induced obesity. *J Bone Miner Res* **2009**, 24, 50-61.
62. Lee, J.; Guarino, V.; Gloria, A.; Ambrosio, L.; Tae, G.; Kim, Y. H.; Jung, Y.; Kim, S. H. Regeneration of Achilles' tendon: the role of dynamic stimulation for enhanced cell proliferation and mechanical properties. *J Biomater Sci Polym Ed* **2010**, 21, 1173-90.
63. Jung, Y.; Kim, S. H.; Kim, Y. H.; Xie, J.; Matsuda, T.; Min, B. G. Cartilaginous tissue formation using a mechano-active scaffold and dynamic compressive stimulation. *J Biomater Sci Polym Ed* **2008**, 19, 61-74.
64. Jung, Y.; Kim, S. H.; Kim, Y. H. The effects of dynamic and three-dimensional environments on chondrogenic differentiation of bone marrow stromal cells. *Biomed Mater* **2009**, 4, 055009.